https://doi.org/10.1016/j.ymssp.2018.03.012

External force estimation of a piezo-actuated compliant mechanism based on a fractional order hysteresis model

Zhiwei Zhu [a], Suet To [b,†], Yangmin Li [c], Wu-Le Zhu [d], and Leixiang Bian [a]

a. School of Mechanical Engineering, Nanjing University of Science and Technology, Nanjing, J.S. 210094, China

b. State Key Laboratory of Ultra-precision Machining Technology, Department of Industrial and Systems Engineering, The Hong Kong Polytechnic University, Kowloon, Hong Kong SAR, China

c. Department of Industrial and Systems Engineering, The Hong Kong Polytechnic University, Kowloon, Hong Kong SAR, China

d. Department of Micro-Engineering, Kyoto University, Nishikyo-ku, Kyoto, 615-8540, Japan

† *Corresponding author: sandy.to@polyu.edu.hk*

Abstract

Sensing of external forces applied on piezo-actuated compliant mechanisms plays a key role in state monitoring, process control and feedback strategy design in a variety of fields, including micro-/nanopositioning, micro-/nanomanipulation, and micro-/nanomanufacturing. In this paper, a force estimation strategy is proposed by comparing the practically measured displacement with the estimated free one without external forces, when subjecting to any given actuation voltages. To have an accurate prediction of the free displacement relating to the actuation voltage, an improved fractional order model is proposed. With this model, the system response is decomposed into a basic linear component and a nonlinear hysteresis component, and the extracted hysteresis is then described by an ordinary fractional order differential model using a modified voltage signal as the model input, which extracts a linear time-delay component from the original voltage. Comparative study with other two differential type hysteresis models are experimentally conducted on a piezo-actuated bridge-type compliant mechanism, demonstrating well the effectiveness and superiority of the proposed model for both system response modeling and external force estimation.

Keywords: Compliant mechanism, piezoelectric actuator, external force estimation, hysteresis nonlinearity, fractional order model.

1. Introduction

Piezo-actuated compliant mechanisms are now used in precision engineering and nanotechnol-ogy related fields, including nanopositioning for micro-/nanoimaging, micro-/nanomanipulation, biomedical micro-/nanodevices, and micro-/nanomanufacturing, to mention a few [1–4]. Sensing external forces applied on the end-effector of the mechanism was demonstrated to play an impor-tant role for interaction perception in these practical applications. For example, the contact force adjustment in micro-/nanomanipulation is critically required to avoid damaging the objects [5, 6], and also, through controlling the cutting force on a piezo-actuated fast tool servo, in-process repositioning of the diamond tool was realized for tool setting [7], as well as for repair of defective microstructures in diamond cutting [8].

Measurement of external forces through embedding force sensors is the most direct way to provide required force signals for any specified processes [6, 7, 9, 10]. However, usage of force sensors will inevitably add extra-costs to the system, and usually, limited bandwidth of the force sensors may block potential applications of the system for high frequency operations [6]. Moreover, for applications of the compliant mechanism with compactness requirement, it is difficult to integrate the force sensor into the system with limited space [9, 10]. Sensorless force estimation is an alternative and very promising solution to capture external forces. With this method, a closed-loop force observer was introduced for external force estimation, which was essentially derived from system model of the piezo-actuated mechanism relating the actuation voltage and output displacement [5]. The term "closed-loop" here means that the practical displacement was required to be captured through the displacement sensor for constructing the force observer. By ignoring the inherent nonlinearity of piezoelectric actuators, the observer can be simply developed from the linear differential equation based on the Newton's second law [5]. Definitely, the unmodeled system nonlinearity (normally 20%of the output displacement) will lead to high estimation error of external forces [11].

As for force estimation, another method using the concept of self-sensing was recently introduced for bimorph actuators to simultaneously estimate both position and force signals without using any sensors [12, 13]. Realization of self-sensing of the two signals relies on the integrated charge as well as the hysteresis force, hence, an integration circuit and a hysteresis model relating the charge and voltage are commonly required. However, due to external disturbances and inevitable saturation effects of the circuit, it is extremely difficult to gain stable and accurate estimation of the desired signals [13, 14]. Therefore, usage of ultraprecision capacitive or laser displacement sensors is still an irreplaceable choice. On the other hand, to construct the "hysteresis force" for external force estimation, the Prandtl-Ishlinkii [12–14] and Bouc-Wen model [11] are employed for the description of the "hysteresis force" during the estimation process. Generally, almost all the developed hysteresis models can be adopted as potential candidates for estimation of the "hysteresis force". With detailed discussions on hysteresis models for piezoelectric actuators, one can refer to recent surveys for detailed discussions [15, 16].

Currently, description of hysteresis is mainly dominated by phenomenological models, which can then roughly classified as operator based, artificial intelligent based, and differential equation based models [15]. The operator based models, such as Preisach model [8, 17] and Prandtl-Ishlinskii model [14, 18], approximate the complex hysteresis by weighting a set of discontinuous elementary operators. However, it is hard to give any general methods to determine the optimal configuration of the operator based models. Artificial intelligent based models commonly possess very high modeling precision for certain particular applications [12, 13], whereas, there is a lack of the capability to completely describe the hysteresis in a general way [15]. With respect to the differential equation based models, they usually employ first-order nonlinear differential equations, such as backlash-like model [12], Bouc-Wen model [11, 19, 20], and Duhem model [15]. However, for both the operator based and differential equation based models, specified improvements are required to compensate

for the inherent asymmetric and rate-dependent properties of the hysteresis to increase the modeling accuracy, generally leading to much higher complexity [18, 20].

Interestingly, the fractional order calculus was recently introduced for the modeling of hysteresis, and a simple ordinary linear fractional order differential model (LFDM) [21] and a fractional order Maxwell resistive capacitance (MRC) model [22] were reported. It is reported that the employment of fractional order operator in the two models can lead to the capability to capture the rate-dependent feature of hysteresis [21, 22]. The two models may belong to the differential equation based hysteresis models, or more accurately, they are the extended ones due to the fact that the differential order is extended from integers to be arbitrary real numbers. In general, the LFDM employed a differential model to simultaneously describe both the linear and nonlinear components of system responses, resulting in limited accuracy and flexibility for modeling actuations with more complicated wave shapes. Meanwhile, the fractional order MRC model adopted the fractional order element as the basic operator, and summarization of a set of these elements may lead to much larger computational burden. However, the unique nonlocal memory effect as well as high flexibility of fractional order calculus provides an excellent background for the application for the modeling of hysteresis [21, 22].

In this paper, a force observer is established for the estimation of external forces on a piezo-actuated compliant mechanism. The core of the observer is an improved fractional order model (IFM) for accurate description of system responses with respect to actuation voltages. With the IFM, system response of piezoelectric actuators is decomposed into a basic linear and a nonlinear hysteresis components. Although the nonlinear component is described through an ordinary frac-tional order differential model, extraction of a linear time-delay voltage from the original command is adopted as the input excitation of the IFM, which may greatly enhance the modeling perfor-mance for hysteresis. Experimental demonstration of both the improved hysteresis model and the

force estimation strategy is conducted with further comparative studies with that using other two differential models.

2. Principle of external force estimation

Considering a typical piezo-actuated compliant mechanism for closed-loop nanopositioning, the corresponding block diagram is shown in Fig. 1(a). The actuation voltage $u(t)$ on the actuator and the external force $f(t)$ on the end-effector of the mechanism jointly lead to an output displacement of $x(t)$. The compliant mechanism works in the elastic deformation region and obeys the linear Hook's law, whereas, the piezoelectric actuator suffers from the complex nonlinearity induced from internal frictions.

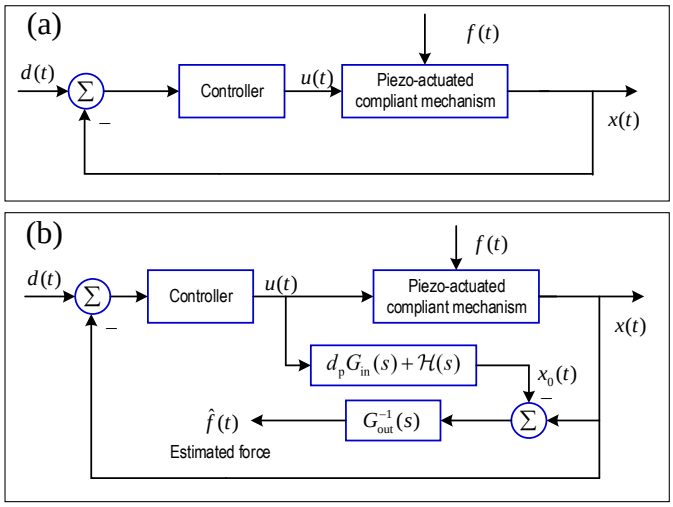

Figure 1: System schematic of (a) the typical piezo-actuated compliant mechanism, and (b) the principle for external force estimation, where $d(t)$ denotes the desired trajectory.

2.1. Force estimation

The basic principle for force estimation is illustrated in Fig. 1 (b). With consideration of the actuation voltage $u(t)$ and external force $f(t)$, the output displacement of the mechanism can be

expressed in the s-domain by [5, 23]

$$X(s) = d_{\mathrm{p}} G_{\mathrm{in}}(s) U(s) + \mathcal{H}(s) U(s) + G_{\mathrm{out}}(s) F(s) \tag{1}$$

where s is the Laplace operator, and d_{p} is the piezoelectric constant. $X(s)$, $U(s)$, and $F(s)$ denote the Laplace transformations of the output displacement, the input voltage and the external force, respectively. In addition, $G_{\mathrm{in}}(s)$ and $G_{\mathrm{out}}(s)$ are the transfer functions related the displacement of the end effector to the input voltage and external force, respectively. $\mathcal{H}(s)$ is the lumped transfer function for the description of the hysteresis effect.

Generally, when actuation voltages and external forces are relatively smooth, and the contained frequencies are well below the natural frequency of the piezo-actuated mechanism, the transfer functions $G_{\mathrm{in}}(s)$ and $G_{\mathrm{out}}(s)$ can be simplified as $G_{\mathrm{in}}(s) = k_{\mathrm{in}}^{-1}$ and $G_{\mathrm{out}}(s) = k_{\mathrm{out}}^{-1}$, where k_{in} and k_{out} denote the input and output stiffness of the mechanism. Therefore, as shown in Fig. 1(b), the external force can be estimated by

$$F(s) = k_{\mathrm{out}} \left[X(s) - X_{\mathrm{o}}(s) \right] \tag{2}$$

$$X_{\mathrm{o}}(s) = d_{\mathrm{p}} k_{\mathrm{in}}^{-1} U(s) + \mathcal{H}(s) U(s) \tag{3}$$

where $X_{\mathrm{o}}(s)$ is the Laplace transformation of the free displacement at the end-effector in absence of external forces. Since the actual displacement can be captured by a capacitive sensor, the free displacement $X_{\mathrm{o}}(s)$ induced by the voltage $U(s)$ is required to be accurately estimated to reconstruct external forces.

Taking inverse Laplace transformation of Eq. (2) leads to the estimated external force in the

time domain by

$$\hat{f}(t) = k_{\text{out}} \left[x(t) - x_{\text{o}}(t) \right] \tag{4}$$

where $f(t)$ and $x_{\text{o}}(t)$ denote the estimated force and free displacement, respectively.

2.2. Free displacement estimation

Estimation of the free displacement is to relate output displacements to input commands of the flexure mechanism, and the key issue is to accurately model the inherent nonlinear hysteresis of the piezo-actuator. To better capture the rate-dependent and non-local memory effects, a new fractional order model is developed with significant improvement from the LFDM reported in Ref.[21].

2.2.1. LFDM for hysteresis

With the LFDM in Ref. [21], the relationship in Eq. (3) was directly modified to be an ordinary linear fractional order differential equation to describe the hysteresis between $X_{\text{o}}(s)$ and $U(s)$. As for the fractional order MRC model introduced in Ref. [22], although the modeling frame was a bit different, the basic operation relating the charge and voltage used similar first order differential equation.

Essentially, the LFDM is a fractional order Kelvin-Voigt model for modeling stress-strain behavior of viscoelastic materials [24, 25], and it can be expressed in the s-domain by

$$X_{\text{o}}(s) + c_0 s^{\beta_0} X_{\text{o}}(s) = a_0 U(s) + b_0 s^{\alpha_0} U(s) \tag{5}$$

Accordingly, through solving the LFDM in Eq. (5), the free displacement can be obtained as

$$X_{\text{o}}(s) = \frac{a_0 + b_0 s^{\alpha_0}}{1 + + c_0 s^{\beta_0}} U(s) \tag{6}$$

where $\alpha_0 \in (0, 1)$ and $\beta_0 \in (0, 1)$ are the differential orders, and a_0, b_0, and c_0 are material property related constants.

2.2.2. Improved fractional order model for hysteresis

With the model described in Eq. (5), it treats the output displacement as a single component and tries to approximate both the linear and nonlinear responses simultaneously. Generally, output displacement of a piezoelectric actuator can be regarded as a combination of two components, including one linear part relating the basic linear response from the input voltage, and another nonlinear part describing the inherent hysteresis [26–28]. Therefore, a separation of linear and nonlinear components is employed herein, and the relationship in Eq. (3) is accordingly modified to be

$$X_{\mathrm{o}}(s) - d_{\mathrm{p}} k_{\mathrm{in}}^{-1} U(s) = \frac{a + bs^{\alpha}}{1 + cs^{\beta}} U_{\mathrm{d}}(s) \tag{7}$$

where α and β are the fractional orders, and a, b, and c are material property related constants contributed to the hysteresis nonlinearity. $U_{\mathrm{d}}(s)$ is a modified input voltage for the IFM.

As shown in Eq. (7), the left side of the equation contains two terms, showing the extraction of a pure linear component related to the input voltage from the nonlinear output. It would be a better choice to make $U_{\mathrm{d}}(s)$ have similar features. Therefore, a linear time-delayed term is introduced to partially simulate the nonlinear hysteresis, and the term $U_{\mathrm{d}}(s)$ can be accordingly expressed by

$$U_{\mathrm{d}}(s) = U(s)e^{-\tau s} - U(s) \tag{8}$$

In the time domain, the term, s^{α} for example, can be represented by the operator ${}_0\mathcal{D}_t^{\alpha}(\cdot)$, showing differential operation with a fractional order α from initial time 0 to t. Using this operator,

taking inverse Laplace transformation of Eq. (7) yields

$$c\cdot{}_0\mathcal{D}_t^{\beta}\hbar(t)+\hbar(t)=au_{\mathrm{d}}(t)+b\cdot{}_0\mathcal{D}_t^{\alpha}u_{\mathrm{d}}(t) \tag{9}$$

with

$$\hbar(t)=x_0(t)-d_{\mathrm{p}}k_{\mathrm{in}}^{-1}u(t) \tag{10}$$

$$u_{\mathrm{d}}(t)=u(t-\tau)-u(t) \tag{11}$$

Generally, there are two definitions for fractional calculus, namely the Grunwald-Letnikov (G-L) definition and the Riemann-Liouville (R-L) definition [25, 29]. To carry out direct numerical solution of Eq. (9), the G-L definition is adopted. As for a function of $g(t)$, the corresponding differential operation with an order of $\mu\in(0,1)$ can be expressed by [29]

$${}_0\mathcal{D}_t^{\mu}g(t)=\lim_{p\to 0}\frac{1}{p^{\mu}}\sum_{k=0}^{t/p}\omega_k^{(\mu)}g(t-kp) \tag{12}$$

where p is the discrete step-size, and $\omega_k^{(\mu)}$ can be recursively derived by

$$\omega_k^{(\mu)}=\left(1-\frac{\mu+1}{k}\right)\omega_{k-1}^{(\mu)},\ \omega_0^{(\mu)}=1 \tag{13}$$

Following the G-L definition, Eq. (9) can be expanded to be:

$$\left(1+\frac{c}{p^{\beta}}\right)\hbar(t)+c\cdot{}_0\mathcal{D}_t^{\beta}\hbar(t-p)=au_{\mathrm{d}}(t)+b\cdot{}_0\mathcal{D}_t^{\alpha}u_{\mathrm{d}}(t) \tag{14}$$

Substituting Eq. (12) into Eq. (14), a closed form numerical solution to $\hbar(t)$ can be expressed

by

$$\hbar(t) = \frac{p^{\beta}}{p^{\beta}+c}\left[au_{\mathrm{d}}(t) + \frac{b}{p^{\alpha}}\sum_{k=0}^{t/p}\omega_k^{(\alpha)}u_{\mathrm{d}}(t-kp) - \frac{c}{p^{\beta}}\sum_{m=1}^{t/p}\omega_l^{(\beta)}\hbar(t-mp)\right],\ \hbar(0)=0 \tag{15}$$

As shown in Eq. (15), the calculation requires all the history states of the process. With the increase of time t, the required storage memory and calculation burden will accordingly increase. To make the calculation practical, the short memory principle [25, 29] is also adopted by replacing the term t/p to be t_{s}/p in Eq. (15), where t_{s} denotes a large enough memory length for the calculation. Moreover, the calculation precision is highly dependent on the step-size which is usually the sample period for practical applications [29]. Therefore, relatively large sampling ratio is required to get reliable results.

After obtaining $\hbar(t)$, the external force can be estimated by substituting Eq. (10) and Eq. (15) into Eq. (4), leading to:

$$\hat{f}(t) = k_{\mathrm{out}}\left[x(t) - \hbar(t) - d_{\mathrm{p}}k_{\mathrm{in}}^{-1}u(t)\right] \tag{16}$$

It is noteworthy that the term $x_0(t) = \hbar(t) + d_{\mathrm{p}}k_{\mathrm{in}}^{-1}u(t)$ describes responses of piezoelectric actuators with consideration of the inherent hysteresis nonlinearity well. The two terms $\hbar(t)$ and $d_{\mathrm{p}}k_{\mathrm{in}}^{-1}u(t)$ also show the relative ratio between the nonlinear and linear components contributing to the final outputs, and the ratio is essentially determined by inherent properties of piezoelectric materials. With respect to different working conditions, slight variation of the practical output can be better estimated by linearly setting $\hat{x_0}(t) = \kappa x_0(t) + \chi$, and the two constants κ and χ can be simply identified through linear least square method.

Remark 1. The hysteresis term $\hbar(t)$ shown in Eq. (15) suggests that it not only depends on the current actuation voltage, but also depends on all of its previous states. This nonlocal effect of

fractional order calculus is essentially beneficial for the description of the inherent memory effect as well as rate-dependent property of the hysteresis of piezoelectric actuators.

Remark 2. Essentially, the proposed IFM belongs to the differential equation based modeling method [19]. However, the proposed model extends the differential order from particular inte-ger number to be arbitrary real number, making it a more natural and more flexible way for process modeling. Meanwhile, the continuous and simple scheme of the fractional order equation leads to an explicit solution, which is usually difficult to obtain by existing models.

Remark 3. Compared with the LFDM introduced in Ref. [21], detraction of the linear component $d_{\mathrm{p}}k_{\mathrm{in}}^{-1}u(t)$ from $x_0(t)$ makes the fractional order model concentrate more on direct modeling of the hysteresis nonlinearity $\hbar(t)$. Moreover, detraction of the linear time-delay component from the input voltage, which adopts the linear time-delay system to partially simulate the nonlinear hysteresis, may also contribute to shape conformal for the model input $u_{\mathrm{d}}(t)$ with respect to the hysteresis$\hbar(t)$.

Remark 4. Although the proposed force estimation method is demonstrated through a single axis piezo-actuated compliant mechanism, it is also effective for other multi-axial piezo-actuated mechanisms by combining the corresponding well modeled kinematics.

3. Parameter identification

3.1. Problem statement

As shown in Eq. 4, the external force linearly relates the displacement of the end-effector by a factor of output stiffness which can be easily identified through the calibration process. To have an accurate estimation of external forces, the key issue is to find a proper set of parameters to minimize the deviation between modeled and practically captured free displacements, i.e. $\hat{x}_0(t)$ and $x_0(t)$,

respectively. Herein, the root-mean-square error is employed as the objective function for reflecting the modeling deviation.

In detail, the identification problem can be summarized as follows:

1. Objective function:
$$\min \ rms = \sqrt{\frac{1}{N}\sum_{m=1}^{N}\left[\hat{x}_0(m) - x_0(m)\right]^2} \tag{17}$$
2. Variables: $\mathbf{P} = [a, b, c, \alpha, \beta, \tau, \Delta]$, where $\Delta = d_{\mathrm{p}} k_{\mathrm{in}}$.
3. Subject to: the upper and lower boundaries of the parameters are set as $\mathbf{P}_{\min} = \mathbf{O}$, and $\mathbf{P}_{\max} = [1, 1, 10, 10, 10, 10, 10]$

As shown in Eq. (10) and Eq. (15), there are seven key parameters to be identified to minimize the objective function in Eq. (17). In general, it is a multi-dimensional minimization problem with high nonlinearity. Although the high nonlinearity and high dimensionality imposes tough challenges for the solving of the minimization problem, the evolutionary computation based methods, including the genetic algorithm (GA) [30], the particle swarm optimization (PSO) [18] and the differential evolution (DE) based algorithms [19, 31], to mention a few, have been proved to have high capability for finding the solutions.

Without loss of generality, a typical DE algorithm featuring simple evolutionary scheme and few tunable parameters [32, 33] is adopted to solve the minimization problem as stated above, so as to identify parameters of the proposed IFM.

3.2. Identification results

With the identification, a harmonic signal with nonlinearly varied amplitude is employed as the actuation voltage $u(t)$. The practical mechatronic system for implementing the actuation and measurement process will be described in section 4.1. It results in the output displacement $x_0(t)$ as

shown in Fig. 2 (a). Based on the actuation $u(t)$ and the captured displacement $x_0(t)$, the model parameters are accordingly determined as $\hat{\mathbf{P}} = [5.7342, 6.8754, 0.8885, 0.6596, 0.9742, 0.0015, 1.7615]$.

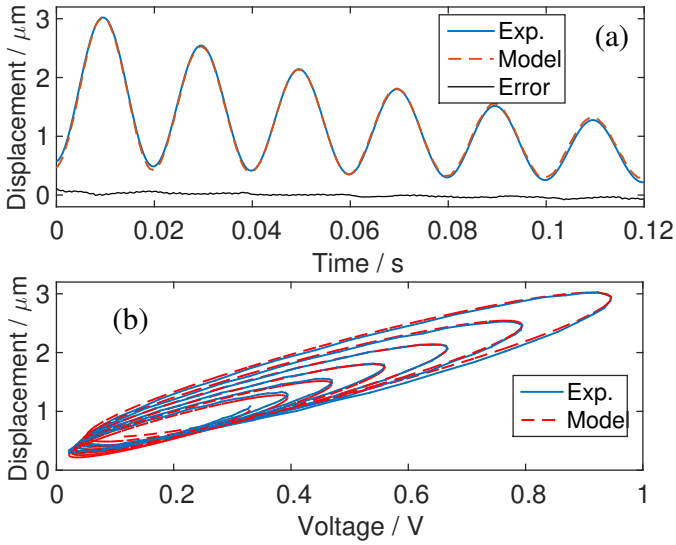

Figure 2: Practical and modeled system responses using the identified parameters, (a) responses in the time domain, and (b) the corresponding hysteresis loops.

Using the identified parameters, the corresponding model output and the modeling error are then illustrated in Fig. 2 (a). The modeling error appears to have a peak-to-valley (PV) value of about 0.06 μm, which is about 2% of the full span of the output displacement. Furthermore, relationship between the actuation voltage and both the practical and modeled outputs are shown in Fig. 2 (b). Good agreement between the practical and modeled hysteresis loops demonstrates the effectiveness of the proposed identification method well.

4. Experimental verification

In this section, detailed experimental testing is further conducted to demonstrate capability of the proposed IFM for the description of hysteresis of piezoelectric actuators, and also to verify the effectiveness of the proposed method for the estimation of external forces. Based on a especially designed bridge type compliant mechanism (BTCM) with structural symmetry, the intermediate variable $x_o(t)$ is indirectly captured from the counterpart of the end-effector by a capacitive dis-

placement sensor for the verification process.

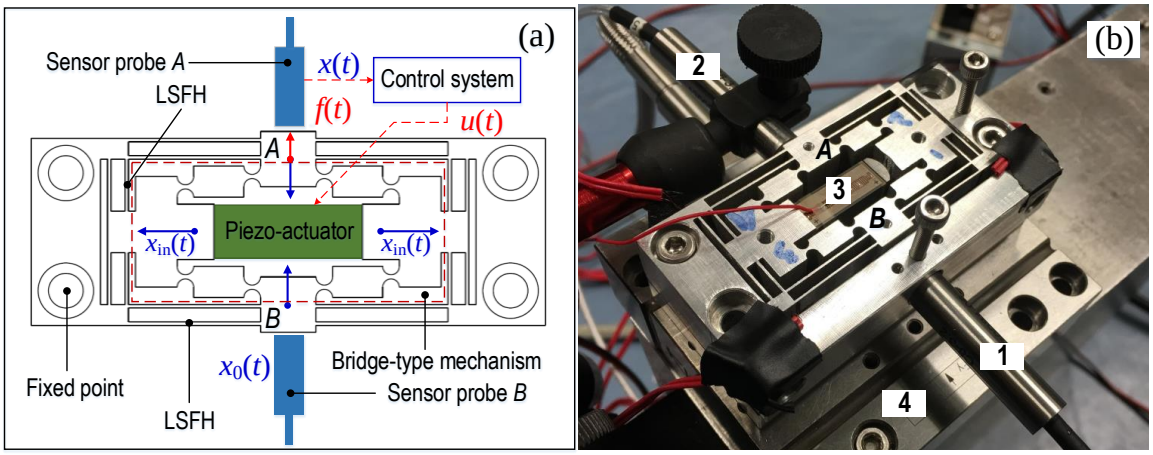

Figure 3: The mechatronic system for experimental testing, (a) Schematic of the piezo-actuated mechatronic system, and (b) the photography of the testing system with 1. sensor probe A, 2. sensor probe B, 3. the piezoelectric actuator, and 4. the dynamometer.

4.1. The mechatronic system

The schematic of the designed BTCM which has two input and two output ends is illustrated in Fig. 3 (a), and a photograph of the practical system fixed on a three-axis dynamometer (Kistler 9255b, Germany) is shown in Fig. 3 (b). Unlike conventional application of the BTCM, four sets of parallelogram structures with each consisting of four typical leaf spring flexdure hinges (LSFH) are adopted to guide motions of all the input and output ends. During testing, one piezoelectric actuator (PI P-880.51, Germany) is actuated through a power amplifier (PI E617.001, Germany) with a gain of 10 ± 0.1 to generate the symmetric input displacements $x_{\text{in}}(t)$ at the two input ends. The outputs amplified through the bridge structure are then captured by two capacitive displacement sensors (Elite, Lion Precision, USA), namely the sensor probes A and B as shown in Fig. 3. Through swept excitation, the natural frequency of the mechanism is obtained to be about 3.4 kHz with relatively flat frequency response below 1 kHz.

During actuation, the captured displacement from probe A is adopted as the feedback signal and transferred to the control board (Power PMAC, Delta Tau Data Systems, Inc., USA) for the

calculation of the actuation voltage $u(t)$. Suffering from the actuation voltage $u(t)$ and external force $f(t)$, the output displacement of the end-effector A is obtained as $x(t)$, tracking the desired trajectory $d(t)$. Without loss of generality, a typical Proportion-Integration-Differentiation (PID) controller with parameters tuned by trail-and-error method is employed herein for the closed-loop control.

Taking advantage of the total symmetry of the designed BTCM, the intermediate free displacement $x_0(t)$ subjecting to $u(t)$ can be observed simultaneously by measuring practical motion of the end-effector B for the model verification. Moreover, to verify the force estimation capability, a random external force $f(t)$ is manually imposed on the end-effector A, and then captured through the dynamometer as shown in Fig. 3 (b).

4.2. Hysteresis response verification

The core component for the force observer is the relationship between the input voltage $u(t)$ and the free displacement $x_0(t)$ with consideration of the hysteresis nonlinearity. Therefore, a comprehensive assessment of the proposed IFM is firstly conducted. To evaluate the capability of the IFM for modeling rate-dependent hysteresis, a complex composition signal with combination of five harmonic signals using different frequencies (5 Hz, 10 Hz, 15 Hz, 20 Hz, and 30 Hz) and phases is adopted as the actuation voltage. Both practical and modeled system responses in the time domain are illustrated in Fig. 4 (a), showing good agreement with each other. Moreover, as shown in Fig. 4 (b), the practical hysteresis loop is in good accordance with the modeled one, irrespective to major or minor loops. This demonstrates that the proposed IFM has good capability to capture the dynamic feature of the hysteresis.

To demonstrate the advantage of the proposed IFM for hysteresis modeling, the popular Bouc-

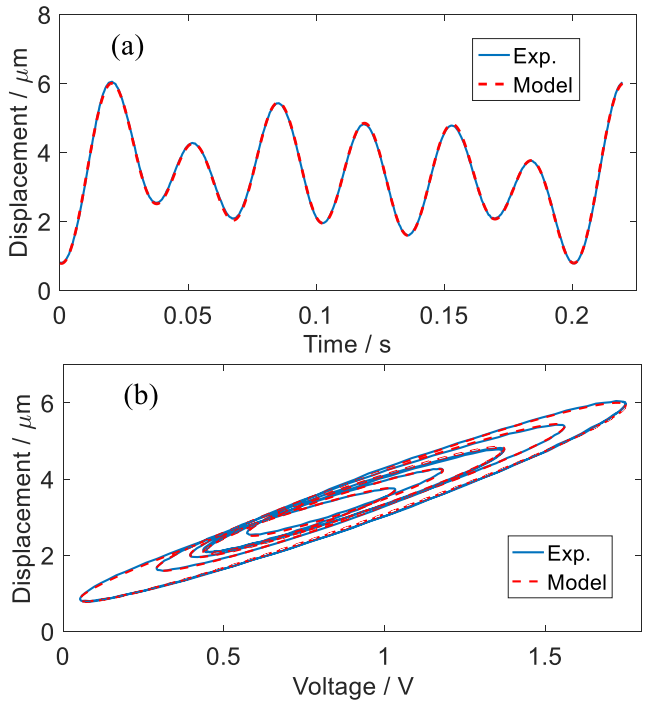

Figure 4: Practical and modeled system responses to a complex composition signal, (a) the displacements in the time domain, and (b) the hysteresis loops.

Wen model (BWM) is employed for comparison study, which is mathematically expressed by [34]:

$$\begin{cases} x_o(t) = d_{\mathbf{p}} u(t) - h_{\mathrm{b}}(t) \\ \dfrac{\mathrm{d}h_{\mathrm{b}}}{\mathrm{d}t} = A_{\mathrm{b}} \dfrac{\mathrm{d}u}{\mathrm{d}t} - B_{\mathrm{b}} \left| \dfrac{\mathrm{d}u}{\mathrm{d}t} \right| h_{\mathrm{b}} - \Gamma_{\mathrm{b}} \dfrac{\mathrm{d}u}{\mathrm{d}t} \left| h_{\mathrm{b}} \right|, \ h_0 = 0 \end{cases} \tag{18}$$

Moreover, the LFDM in Eq. (5) as introduced in [21] is also adopted for comparison. Following the same identification procedures in section 3.1, the identified four parameters for the BWM are $A_{\mathrm{b}} = 0.971$, $B_{\mathrm{b}} = 1.486$, $\Gamma_{\mathrm{b}} = 1.97 \times 10^{-7}$, and $d_{\mathbf{p}} = 1.910$. Meanwhile, parameters for the LFDM are $a_0 = 6.573$, $b_0 = 1.459$, $c_0 = 0.198$, $\alpha_0 = 0.176$, and $\beta_0 = 0.466$.

To avoid repetition, only the modeled hysteresis loops resulting from the BWM and the IFM are depicted in Fig. 5 (a), together with the practical loop. Compared with the hysteresis loops in Fig. 4 (c) obtained by the IFM, relatively large deviation between the practical and modeled loops is observed for the LFDM, especially for the minor loops. With the loop generated by the BWM,

a much larger deviation is observed due to the static nature of the BWM.

Modeling errors for the IFM, BWM, and LFDM are further collected in Fig. 5 (b). PV values of the estimated errors for the three models are about 0.12 μm, 0.23 μm, and 0.56 μm, respectively. In general, the modeling error generated by the BWM is about twice of that generated by the LFDM, and nearly 5 times of that generated by the IFM. The much smaller modeling error obtained by the IFM (about 1.94% of the full displacement) suggests that the IFM is capable of accurate description of hysteresis nonlinearity with rate-dependent effects, and it is also more flexible to describe response behavior of piezoelectric actuators subjected to voltages with complicated wave shapes. More importantly, this suggests that a reliable prediction of the free displacement can be achieved to estimate external forces under variable working conditions.

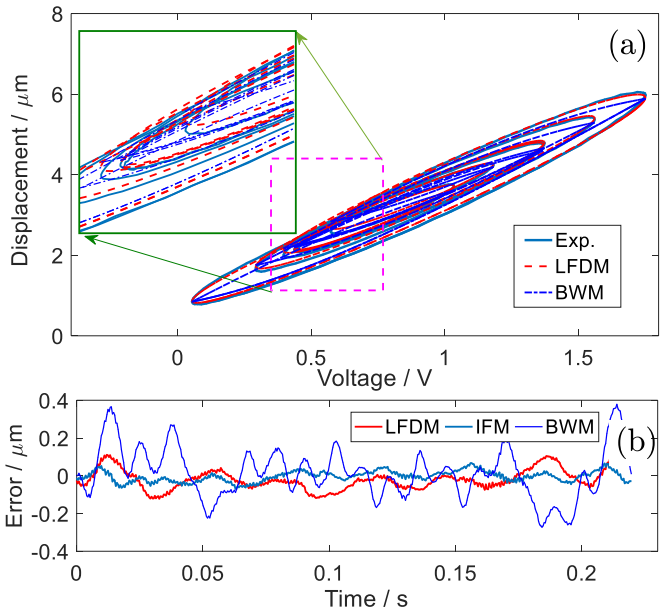

Figure 5: Modeling results using the relationship in Eq. **??**, (a) the hysteresis loops with a partially enlarged view, and (b) the modeling error.

4.3. External force estimation verification

In closed-loop working condition, a random force is manually imposed on the end-effector A along the working motion direction which tries to follow a harmonic trajectory with 2 μm amplitude

and 3 μm offset. The resulted following results with force disturbances are illustrated in Fig. 6 (a), showing good tracking performance with small following error. To have a good resistance to external disturbance, an extra amount of voltage is required to implement on the piezoelectric actuator, resulting in the observed non-harmonic free displacement measured from the counterpart end-effector B as illustrated in Fig. 6 (b). The modeled output subjected to the practical voltage is also illustrated in Fig. 6 (b), showing good agreement with the measured one. The modeling error is about 0.256 μm which is about 5.45% of the full displacement. The error ratio is much higher than that obtained in section 4.2. In this case, the free displacement is indirectly observed from the end-effector B. Any inconsistence of the two ends such as structure parameter differences induced by manufacturing errors and non-symmetric driving induced by assembly errors of the actuator may lead to parameter changes of the model, and accordingly lead to higher modeling errors as observed.

Following the relationship shown in Eq. (4), the estimated force is obtained and calibrated by having a comparison with the practical force captured from the dynamometer. The output stiffness is then determined as $k_{\text{out}} = 1.08\ N/\mu m$. The estimated and practical forces are illustrated in Fig. 6 (c) . To have a view of more detailed features, an enlarged view from $t = 14\ s$ to $t = 19\ s$ is further given in Fig. 7 (a). Good accordance of even very detailed features between the practical and estimated forces are observed, showing the effectiveness of the proposed method for estimating external forces.

To have a comparison with other modeling methods, enlarged views of the estimated forces obtained through both the BWM and LFDM are also illustrated in Fig. 7 (a). The observed larger deviations demonstrate the poor estimation capability through usage of the two models. The estimated force errors by adopting the three models are further shown in Fig. 7 (b). The error obtained through the IFM is observed to be about $\pm 0.039\ N$, and the errors by adopting the BWM and LFDM are about $\pm 0.18\ N$ and $\pm 0.28\ N$, respectively. Since the external force is highly random

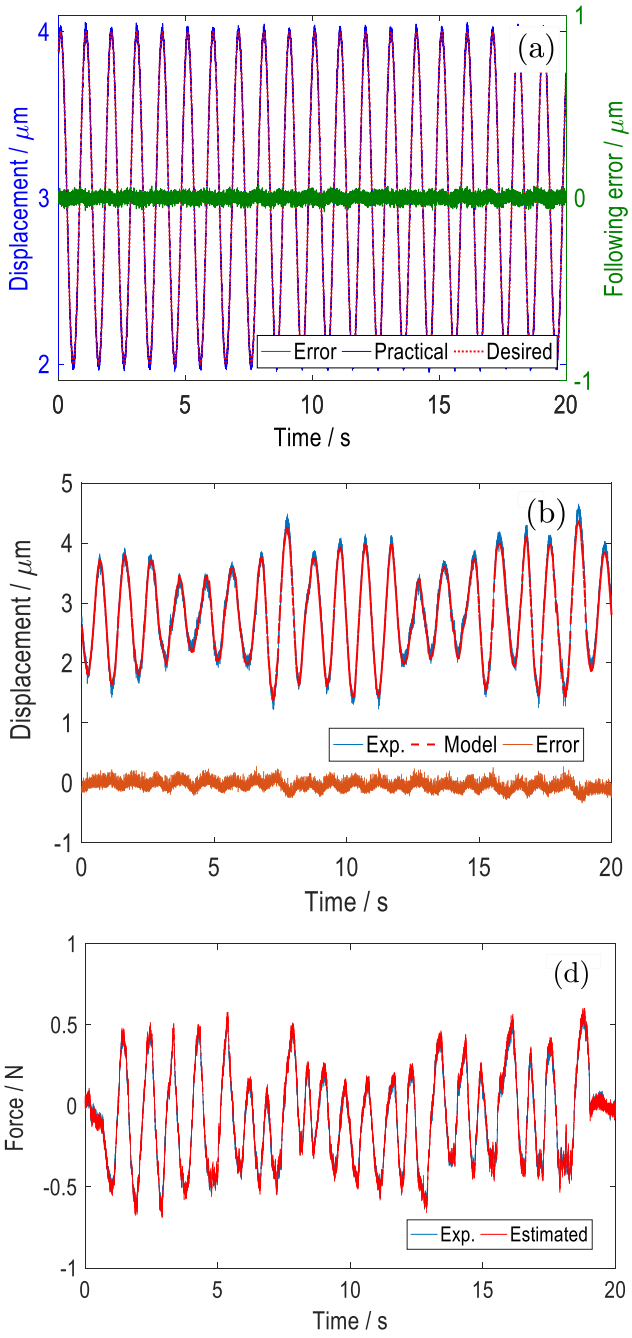

Figure 6: System responses under external forces, (a) tracking performance of the motion of the end-effector A, (b) the resulting practical and modeled responses at the end-effector B with the modeling error, (c) the practical and estimated external forces.

with intensive rate variations, the relatively large estimation errors obtained by using the BWM and LFDM may attribute to their limited modeling capability for rate-dependent hysteresis. In contrast, it further demonstrates the superiority of the proposed method using IFM for capturing

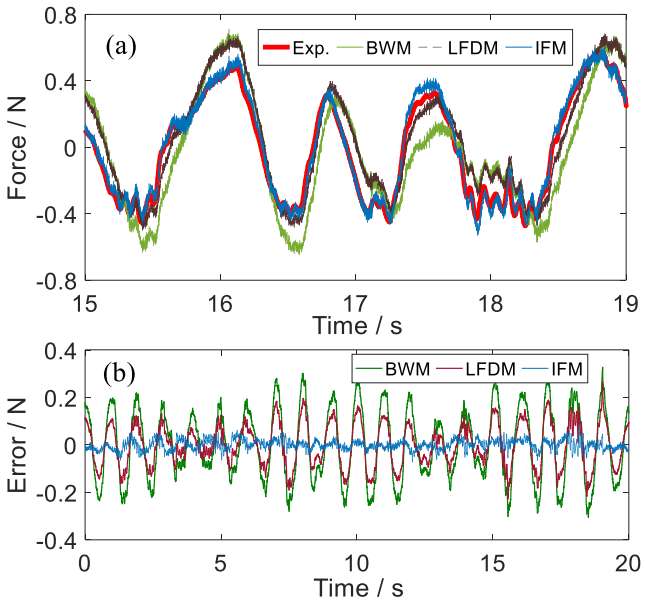

Figure 7: Estimation results of external forces, (a) enlarged view of the practical and estimated forces from $t = 14s$ to $t = 19s$, and (b) estimation errors of forces obtained by different models from initial time to the end.

external forces under different working conditions.

5. Conclusion

External forces on end-effectors of piezo-actuated compliant mechanisms were proposed to be estimated by comparing the practical output displacement suffering from external forces with the free one obtained without forces under the same actuation condition. To accurately estimate the free displacement, an improved fractional order model (IFM) is proposed with careful consideration of the inherent hysteresis nonlinearity of piezoelectric actuators. To gain high flexibility and high accuracy, the displacement was decomposed into a linear component and a nonlinear component relating the hysteresis effects. The hysteresis component was then independently modeled through a fractional order differential model, using a modified voltage with extraction of a linear time-delayed component as the model input.

Through differential evolution based minimization, parameters for the proposed IFM were optimally identified through system responses to a harmonic actuation signal with nonlinearly varied

amplitudes. By means of a complex composition signal with multiple frequencies, the identified IFM was comprehensively examined and compared with other two reported differential type hysteresis models. Much smaller modeling error demonstrates the flexibility and superiority of the IFM for accurate description of rate-dependent hysteresis under various working conditions.

By manually imposing the random force on the end-effector under closed-loop condition, the measured force through a dynamometer and the estimated force were demonstrated to have good agreement with each other, even with the remote detailed features. Moreover, the estimated error of external force through the IFM is only about $\pm 0.039\ N$, which is much smaller than that obtained by the other two models. It demonstrates that the proposed method using the IFM can accurately estimate external forces more effectively.

Acknowledgments

This work was jointly supported by the National Natural Science Foundation of China (51705254, 51675455), the Natural Science Foundation of Jiangsu Province (BK20170836), and the Fundamental Research Funds for the Central Universities (30917011301, 309171A8804).

References

[1] Y. Li, Q. Xu, A novel piezoactuated xy stage with parallel, decoupled, and stacked flexure structure for micro-/nanopositioning, IEEE Transactions on Industrial Electronics 58 (8) (2011) 3601–3615.

[2] W.-L. Zhu, Z. Zhu, P. Guo, B.-F. Ju, A novel hybrid actuation mechanism based xy nanopositioning stage with totally decoupled kinematics, Mechanical Systems and Signal Processing 99 (2018) 747 – 759.

[3] Z. Zhu, X. Zhou, Z. Liu, R. Wang, L. Zhu, Development of a piezoelectrically actuated two-degree-of-freedom fast tool servo with decoupled motions for micro-/nanomachining, Precision Engineering 38 (4) (2014) 809–820.

[4] G. Hao, A multiaxis, large-output, sensing framework of integrating linear optical encoders for nanopositioning systems, IEEE Sensors Letters 1 (3) (2017) 1–4.

[5] Q. Xu, Precision position/force interaction control of a piezoelectric multimorph microgripper for microassembly, IEEE Transactions on Automation Science and Engineering 10 (3) (2013) 503–514.

[6] Q. Xu, Robust impedance control of a compliant microgripper for high-speed position/force regulation, IEEE Transactions on Industrial Electronics 62 (2) (2015) 1201–1209.

[7] W. Gao, Y.-L. Chen, K.-W. Lee, Y.-J. Noh, Y. Shimizu, S. Ito, Precision tool setting for fabrication of a microstructure array, CIRP Annals-Manufacturing Technology 62 (1) (2013) 523–526.

[8] Y.-L. Chen, S. Wang, Y. Shimizu, S. Ito, W. Gao, B.-F. Ju, An in-process measurement method for repair of defective microstructures by using a fast tool servo with a force sensor, Precision Engineering 39 (2015) 134–142.

[9] D. Wang, Q. Yang, H. Dong, A monolithic compliant piezoelectric-driven microgripper: Design, modeling, and testing, IEEE/ASME Transactions on Mechatronics 18 (1) (2013) 138–147.

[10] Q. Xu, Design and smooth position/force switching control of a miniature gripper for automated microhandling, IEEE Transactions on Industrial Informatics 10 (2) (2014) 1023–1032.

[11] K. Abidi, A. Sabanovic, S. Yesilyurt, Sliding mode control based disturbance compensation and external force estimation for a piezoelectric actuator, in: Advanced Motion

Control, 2004. AMC '04. The 8th IEEE International Workshop on, 2004, pp. 529–534. doi:10.1109/AMC.2004.1297924.

[12] I. A. Ivan, M. Rakotondrabe, P. Lutz, N. Chaillet, Current integration force and displacement self-sensing method for cantilevered piezoelectric actuators, Review of Scientific Instruments 80 (12) (2009) 126103.

[13] M. Rakotondrabe, I. A. Ivan, S. Khadraoui, P. Lutz, N. Chaillet, Simultaneous displacement/force self-sensing in piezoelectric actuators and applications to robust control, IEEE/ASME Transactions on Mechatronics 20 (2) (2015) 519–531.

[14] T. McPherson, J. Ueda, A force and displacement self-sensing piezoelectric mri-compatible tweezer end effector with an on-site calibration procedure, IEEE/ASME Transactions on Mechatronics 19 (2) (2014) 755–764.

[15] G.-Y. Gu, L.-M. Zhu, C.-Y. Su, H. Ding, S. Fatikow, Modeling and control of piezo-actuated nanopositioning stages: a survey, IEEE Transactions on Automation Science and Engineering 13 (1) (2016) 313–332.

[16] V. Hassani, T. Tjahjowidodo, T. N. Do, A survey on hysteresis modeling, identification and control, Mechanical Systems and Signal Processing 49 (1) (2014) 209–233.

[17] S. Shao, M. Xu, S. Zhang, S. Xie, Stroke maximizing and high efficient hysteresis hybrid modeling for a rhombic piezoelectric actuator, Mechanical Systems and Signal Processing 75 (2016) 631 – 647.

[18] G.-Y. Gu, L.-M. Zhu, C.-Y. Su, Modeling and compensation of asymmetric hysteresis nonlinearity for piezoceramic actuators with a modified prandtl–ishlinskii model, IEEE Transactions on Industrial Electronics 61 (3) (2014) 1583–1595.

[19] G. Wang, G. Chen, F. Bai, Modeling and identification of asymmetric bouc–wen hysteresis for piezoelectric actuator via a novel differential evolution algorithm, Sensors and Actuators A: Physical 235 (2015) 105–118.

[20] W. Zhu, X.-T. Rui, Hysteresis modeling and displacement control of piezoelectric actuators with the frequency-dependent behavior using a generalized bouc–wen model, Precision Engineering 43 (2016) 299–307.

[21] Z. Zhu, X. Zhou, A novel fractional order model for the dynamic hysteresis of piezoelectrically actuated fast tool servo, Materials 5 (12) (2012) 2465–2485.

[22] Y. Liu, J. Shan, U. Gabbert, N. Qi, Hysteresis and creep modeling and compensation for a piezoelectric actuator using a fractional-order maxwell resistive capacitor approach, Smart Materials and Structures 22 (11) (2013) 115020.

[23] Q. Xu, A new method of force estimation in piezoelectric cantilever-based microgripper, in: 2012 IEEE/ASME International Conference on Advanced Intelligent Mechatronics (AIM), IEEE, 2012, pp. 574–579.

[24] R. Lewandowski, B. Chorazyczewski, Identification of the parameters of the kelvin–voigt and the maxwell fractional models, used to modeling of viscoelastic dampers, Computers and Structures 88 (1) (2010) 1–17.

[25] I. Podlubny, Fractional differential equations: an introduction to fractional derivatives, fractional differential equations, to methods of their solution and some of their applications, Vol. 198, Academic press, 1998.

[26] J. Yi, S. Chang, Y. Shen, Disturbance-observer-based hysteresis compensation for piezoelectric actuators, IEEE/ASME Transactions on Mechatronics 14 (4) (2009) 456–464.

[27] M. Chen, S. S. Ge, Adaptive neural output feedback control of uncertain nonlinear systems with unknown hysteresis using disturbance observer, IEEE Transactions on Industrial Electronics 62 (12) (2015) 7706–7716.

[28] C.-X. Li, G.-Y. Gu, M.-J. Yang, L.-M. Zhu, High-speed tracking of a nanopositioning stage using modified repetitive control, IEEE Transactions on Automation Science and Engineering 14 (3) (2015) 1467–1477.

[29] Y. Chen, I. Petras, D. Xue, Fractional order control-a tutorial, in: 2009 American control conference, IEEE, 2009, pp. 1397–1411.

[30] J.-L. Ha, Y.-S. Kung, R.-F. Fung, S.-C. Hsien, A comparison of fitness functions for the identification of a piezoelectric hysteretic actuator based on the real-coded genetic algorithm, Sensors and Actuators A: Physical 132 (2) (2006) 643–650.

[31] Y. Zhang, P. Yan, Modeling, identification and compensation of hysteresis nonlinearity for a piezoelectric nano-manipulator, Journal of Intelligent Material Systems & Structures 28 (7).

[32] J. Brest, S. Greiner, B. Boskovic, M. Mernik, V. Zumer, Self-adapting control parameters in differential evolution: a comparative study on numerical benchmark problems, IEEE transactions on Evolutionary Oomputation 10 (6) (2006) 646–657.

[33] R. Storn, K. Price, Differential evolution–a simple and efficient heuristic for global optimization over continuous spaces, Journal of Global Optimization 11 (4) (1997) 341–359.

[34] M. Rakotondrabe, Bouc-wen modeling and inverse multiplicative structure to compensate hysteresis nonlinearity in piezoelectric actuators, IEEE Transactions on Automation Science and Engineering 8 (2) (2011) 428–431.

List of Figures